

Role of quantum correlations in light-matter quantum heat engines

G. Alvarado Barrios,^{1,*} F. Albarrán-Arriagada,¹ F. A. Cárdenas-López,^{1,2} G. Romero,¹ and J. C. Retamal^{1,2,†}

¹*Departamento de Física, Universidad de Santiago de Chile (USACH), Avenida Ecuador 3493, 9170124, Santiago, Chile*

²*Center for the Development of Nanoscience and Nanotechnology 9170124, Estación Central, Santiago, Chile*

(Dated: July 20, 2017)

We study a quantum Otto engine embedding a working substance composed by a two-level system interacting with a harmonic mode. The physical properties of the substance are described by a generalized quantum Rabi model arising in superconducting circuits realizations. We show that light-matter quantum correlations reduction during the hot bath stage and compression stage act as a resource for enhanced work extraction and efficiency respectively. Also, we demonstrate that the anharmonic spectrum of the working substance has a direct impact on the transition from heat engine into refrigerator as the light-matter coupling is increased. These results shed light on the search for optimal conditions in the performance of quantum heat engines.

Keywords: Quantum thermodynamics, quantum heat engines

I. INTRODUCTION

Quantum heat engines (QHEs) [1] differ from classical heat engines in that they contain a quantum coherent working body, and the bounds imposed by quantum mechanics on their performance is a fundamental issue in quantum thermodynamics. They are characterized by three attributes: the working medium, the cycle of operation, and the dynamics of the governed cycle. Amongst the quantum cycles in which the engine may operate we have the Carnot cycle and the Otto cycle, with the quantum Otto cycle being the most widely studied [2–8]. With exception of the quantum Carnot cycle, the performance of the quantum cycle depends on the properties of the working substance, leading to several quantum heat engines proposals, namely, spin 1/2 and three-level systems [3, 9–11], harmonic oscillators [12, 13], and hybrid light-matter systems [14, 15]. In particular, for light-matter systems [14] the performance of the engine has been studied in different coupling regimes, exploring the relationship between quantum coherence and correlations for enhancing work extraction.

A fundamental question within the study of QHEs with a working substance consisting of coupled quantum systems, is the role played by quantum correlations among the constituents on the performance of quantum heat machines. For an appropriately strong coupling it is possible to have non-zero quantum correlations even when the global system is in thermal equilibrium with some reservoir at a given temperature. A first insight into this problem has been given by Zhang et. al. [16] considering two interacting spins in a magnetic field linking the performance of the quantum Otto cycle to the entanglement present in the thermal equilibrium state. Additional efforts to understand this issue has been carried out by changing or generalizing the working substance [14, 17–20]. The main thing we have learned is that the effect of quantum correlations on the performance of quantum heat machines are model dependent.

Among the important things to dilucidate when choosing a working substance are: what is the effect of having the energy

spectrum being degenerate or non-degenerate, the effect of the anharmonicity of the spectrum and the capability of the system for embedding quantum correlations. These are the main issues we address in the present work.

We study a quantum Otto engine with a working substance composed by a two-level system interacting with a harmonic mode described by a generalized quantum Rabi model. Such physical device finds its realization in superconducting circuits [21–26] where the interaction can be engineered to have access to different coupling regimes and different anharmonicities. In particular, we will study how the anharmonic spectrum of the quantum Rabi model [27, 28] explains the change in operation regime as a function of the light-matter coupling. Afterwards, by considering the generalized quantum Rabi model we delve into the relation between the light-matter quantum correlations and the extractable work and efficiency of the engine. We show that contrary to previous works, the difference in quantum correlations between the thermal equilibrium states will not be indicative of the extractable work, instead, it is the quantum correlations reduction in the hot bath stage what can be interpreted as enhancing positive work.

This article is organized as follows, in section II we describe the working substance of our QHE, in section III we describe the quantum Otto cycle in which our QHE operates. In section IV we show the influence of the anharmonicity of the energy spectrum of the working substance on the operation regime of the QHE. In section V and VI we show the relation between the quantum correlation reduction during a thermodynamic process of the cycle and the harvested work and engine efficiency respectively. In section VII we consider an adiabatic process which simplifies a physical implementation of our QHE and study the quantum correlations and harvested work. Finally in section VIII we present our conclusions.

II. THE MODEL

Let us consider a QHE embedding a working substance consisting of a single cavity mode interacting with a two-level system which is described by the generalized quantum Rabi

* Gabriel Alvarado gabriel.alvarado@usach.cl

† Juan Carlos Retamal juan.retamal@usach.cl

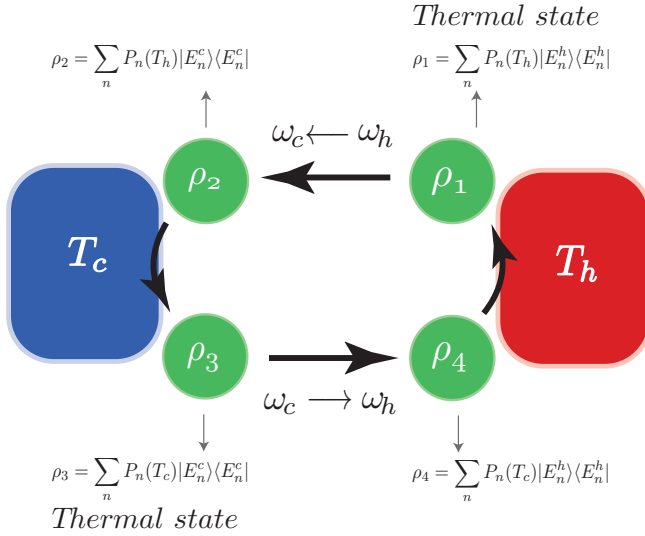


FIG. 1. Diagram of the quantum Otto cycle utilized in this work, we can see the states at the different stages of the cycle. Where T_c and T_h are the temperatures of the cold and hot reservoir, respectively.

model [21–26] :

$$H = \hbar\omega_{\text{cav}}a^\dagger a + \frac{\hbar\omega_q}{2}\sigma^z + \hbar g(\cos(\theta)\sigma^x + \sin(\theta)\sigma^z)(a^\dagger + a). \quad (1)$$

Here, $a(a^\dagger)$ is the annihilation (creation) bosonic operator for the field mode. The operators σ^z and σ^x stand for Pauli matrices describing the two-level system. Also, ω_c , ω_q , g , and θ , are the cavity frequency, qubit frequency, qubit-cavity coupling strength, and mixing angle respectively. In this work we will consider the resonance case for the qubit and cavity frequency $\omega_{\text{cav}} = \omega_q = \omega$.

It is worthwhile to note that for $\theta = 0$, this system corresponds to the quantum Rabi model [27, 28] which has received increasing attention in recent years [29–33]. The ratio of the coupling strength to the resonator frequency g/ω separates the behavior of the system into different regimes [34, 35]. In the strong coupling regime, where the coupling strength is much larger than any decoherence or dephasing rate in the system, and for values $g/\omega \lesssim 10^{-2}$ one can perform the rotating wave approximation (RWA) and the system can be described by the Jaynes-Cummings model [36]. As the ratio g/ω is increased from the strong coupling regime there is a breakdown of the RWA and the system is described by the quantum Rabi model. We distinguish two main regimes for the later model, the ultra-strong coupling regime (USC) [21–23] where the coupling strength is comparable to the resonator frequency $g \lesssim \omega$ and the deep-strong coupling regime (DSC) [24, 37] where the interaction parameter is greater than the relevant frequencies $g \gtrsim \omega$. In both regimes the eigenstates of the model correspond to highly correlated states of the qubit and field mode. In addition the energy spectrum exhibits high anharmonicity as a function of the coupling strength. As we will show later, these properties of the model will explain the transition in operation regime of the quantum heat engine.

III. QUANTUM OTTO CYCLE

In what follows we describe the thermodynamic cycle employed in our QHE. In this work we study a QHE operating under a quantum Otto cycle involving the working substance interacting with a cold and a hot reservoirs through four stages. We will consider that the coupling strength g and the mixing angle θ will be kept constant throughout the cycle. The mode frequency will be changed from ω_h to ω_c to account for the interaction with the hot and cold reservoir respectively. The thermodynamic cycle used in this work is schematically presented in Fig.1:

1. Stage 1: Quantum isochoric process (hot bath stage). The system, with frequency $\omega = \omega_h$ and Hamiltonian H_h is brought into contact with a hot thermal reservoir at temperature T_h until it reaches thermal equilibrium. At the end of this process the state becomes $\rho_1 = \sum_n P_n(T_h) |E_n^h\rangle \langle E_n^h|$, where $\{|E_n^h\rangle\}$ are the eigenstates of Hamiltonian H_h and the corresponding thermal populations $P_n(T_h)$ are given by the Boltzmann distribution for temperature T_h . It is noteworthy that this process will have a specific g/ω_h ratio for a given value of g , because we are fixing the coupling strength g independently from the resonator frequency. During this process only the populations change while the energy level structure remains invariant.
2. Stage 2: Quantum adiabatic (expansion) process. The system is isolated from the hot reservoir, and its frequency is changed from ω_h to ω_c , with $\omega_h > \omega_c$, sufficiently slow as to satisfy the quantum adiabatic theorem such that the populations remain constant throughout the process. During this process only the energy level structure changes. At the end of this process the Hamiltonian is H_c and the state of the system is $\rho_2 = \sum_n P_n(T_h) |E_n^c\rangle \langle E_n^c|$, where the thermal populations are the same as in ρ_1 but the energy eigenstates are those of H_c , therefore the system is no longer in a thermal state.
3. Stage 3: Quantum isochoric process (cold bath stage). The working medium with $\omega = \omega_c$ and Hamiltonian H_c is brought into contact with a cold thermal reservoir at temperature T_c until it reaches thermal equilibrium. The state of the system at the end of this process is given by $\rho_3 = \sum_n P_n(T_c) |E_n^c\rangle \langle E_n^c|$, where $\{|E_n^c\rangle\}$ are the energy eigenstates of H_c and $P_n(T_c)$ are the corresponding thermal populations at temperature T_c . Since the resonator frequency has changed to ω_c due to the adiabatic process, in this stage the ratio g/ω_c for a given value of g is different than in stage 1 as a consequence of the adiabatic process.
4. Stage 4: Quantum adiabatic (compression) process. The system is isolated from the cold reservoir, and its frequency is changed back from ω_c to ω_h . During this process the populations remain unchanged while

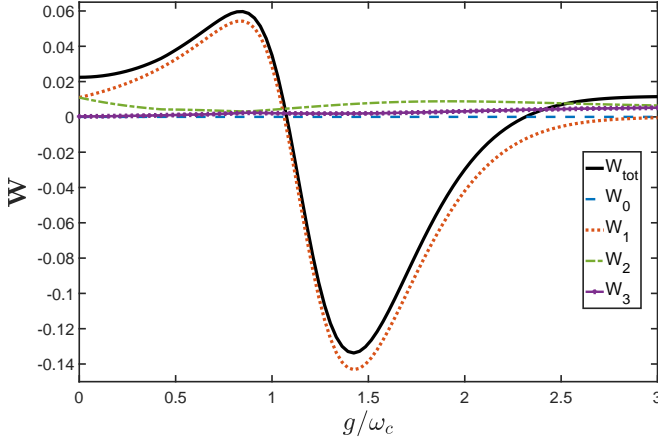


FIG. 2. Work output of the quantum heat engine as a function of the coupling parameter g/ω_c for $\theta = 0$, with $\omega_h = 2\omega$ and $\omega_c = \omega$. We have used temperatures $T_c = 19$ mK and $T_h = 9T_c$.

the energy level structure returns to its configuration in Stage 1. At the end of the process the Hamiltonian is H_h and the state of the system is given by $\rho_4 = \sum_n P_n(T_c) |E_n^h\rangle \langle E_n^h|$, that is, the thermal populations are the same as in state ρ_3 , but the energy eigenstates are those of H_h , thus, this is not a thermal state.

The hot Hamiltonian H_h and the cold Hamiltonian H_c differ only by the frequency of the resonator, either ω_h or ω_c .

We follow the conceptual frame as developed in [38] to define the heat transferred and work performed in a quantum thermodynamics. Let us consider the expectation value of the measured energy of a quantum system with discrete energy levels as given by $U = \langle E \rangle = \sum_n p_n E_n$ where E_n are the energy levels and p_n are the corresponding occupation probabilities. Denote by $dU = \sum_n (p_n dE_n + E_n dp_n)$ as the infinitesimal change of the energy, from which we can obtain the following identifications for infinitesimal heat transferred dQ and work done dW

$$dQ := \sum_n E_n dp_n, \quad dW := \sum_n p_n dE_n. \quad (2)$$

Here the heat transfer is related to the population change dp_n with fixed energy level structure while the work done is related to the change in the energy levels dE_n with fixed populations. The net work done in a single cycle can be obtained from $W = Q_h + Q_c$, where

$$Q_h = \sum_n E_n^h (P_n(T_h) - P_n(T_c)), \quad (3)$$

$$Q_c = \sum_n E_n^c (P_n(T_c) - P_n(T_h)), \quad (4)$$

$$W = \sum_n (E_n^h - E_n^c) (P_n(T_h) - P_n(T_c)). \quad (5)$$

As can be seen in Eq.(5) the work performed by the engine receives a contribution per each energy level, but this contribution will only be relevant if the energy state is sufficiently

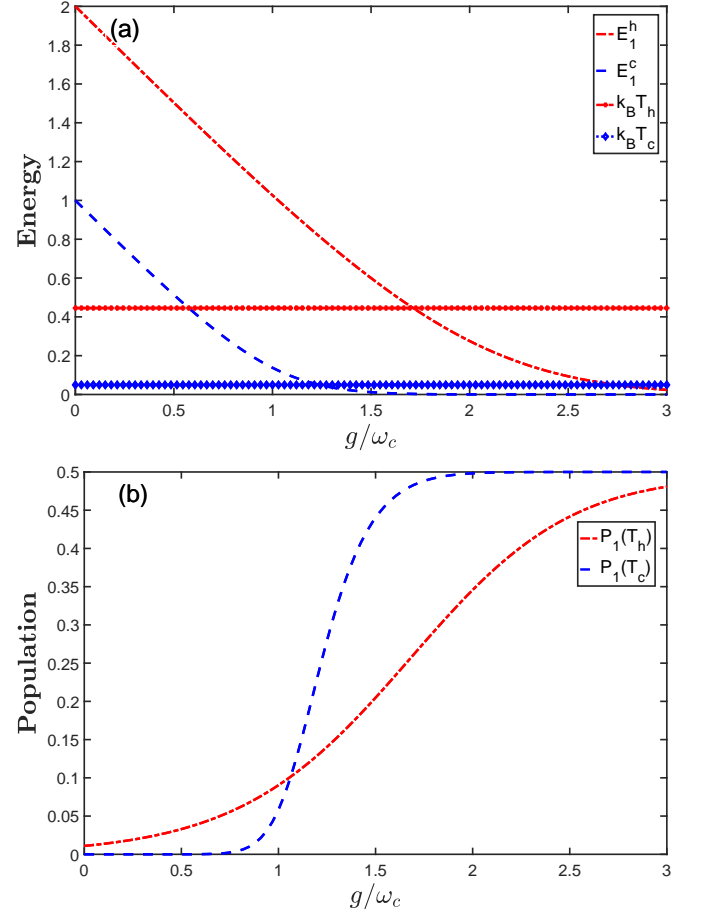


FIG. 3. (a) Energy of the first excited state of the hot and cold Hamiltonian, and the thermal energy of the hot and cold reservoir. (b) Thermal population difference of the first excited state corresponding to the hot and cold Hamiltonians. We have used $\omega_h = 2\omega$, $\omega_c = \omega$ with reservoir temperatures $T_c = 19$ mK and $T_h = 9T_c$.

thermally populated. Let us express the terms of Eq.(5) in the following way

$$W = \sum_n W_n, \quad (6)$$

where

$$W_n = (E_n^h - E_n^c) (P_n(T_h) - P_n(T_c)). \quad (7)$$

Here we call W_n the work contribution of the n -th energy level. Finally, the efficiency of the QHE is defined as the ratio between the extractable work and the heat that enters the system:

$$\eta = \frac{W}{Q_h}. \quad (8)$$

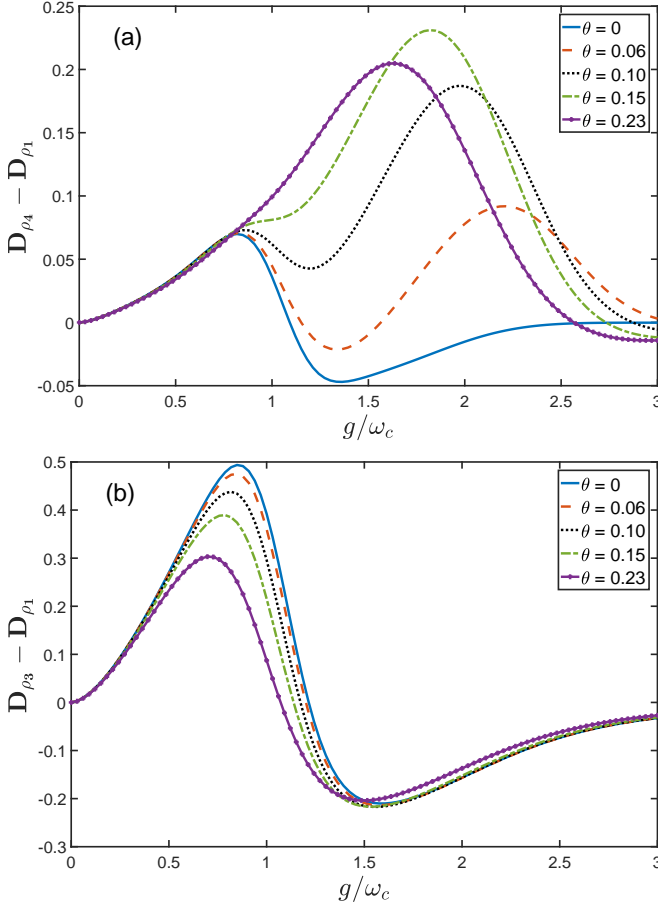


FIG. 4. Difference of quantum correlations between states (a) ρ_4 and ρ_1 which are the initial and final states of the hot bath stage. And (b) states ρ_3 and ρ_1 , which are the cold thermal state and hot thermal state respectively, as a function of coupling parameter g/ω_c for different values of the mixing angle θ . We have used $\omega_h = 2\omega$ and $\omega_c = \omega$, $T_c = 19$ mK and $T_h = 9T_c$.

IV. ANHARMONICITY AND ENGINE OPERATION

It is known that for a working substance described by the quantum Rabi model ($\theta = 0$) the QHE can experience a transition from a heat engine into a refrigerator depending on the light-matter coupling [14]. However it is not yet completely clear what properties of this working substance lead to such behaviour. In this section we show how the anharmonicity and degeneracy of the energy spectrum of the low energy levels of the quantum Rabi model together with the adiabatic process explain this positive to negative work transition.

In Fig. 2 we show the total work output (black line) and the work contribution per energy level W_n for the four lowest states. In this numerical calculation we chose $\omega_h = 2\omega_c$ such that the ratio g/ω of the hot Hamiltonian is half of the ratio of the cold Hamiltonian. The ground state has no contribution on the work extraction so we have $W_0 = 0$, this is because Eq.(5) depends only on the difference of energy levels of H_h and of H_c relative to their own ground state. We can see from Fig. 2 that the main contribution to the total work comes from

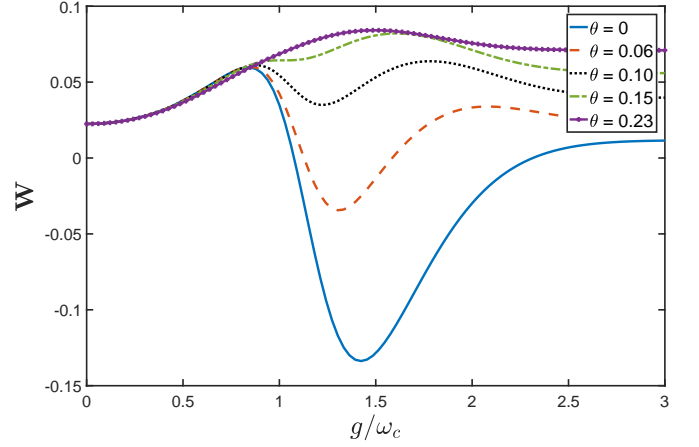


FIG. 5. Work output of the engine versus the interaction parameter g/ω_c for different values of the mixing angle θ . We have used $\omega_h = 2\omega$ and $\omega_c = \omega$, $T_c = 19$ mK and $T_h = 9T_c$.

the first excited state through W_1 , while the second and third excited states have a small and always positive contribution. We see that the change in operation regime from heat engine into refrigerator at $g/\omega_c \lesssim 1.2$ is owed only to the contribution of the first excited state. In addition, at $g/\omega_c > 2.5$ the work contribution of the first excited state W_1 decreases to zero while the contributions of the second and third excited states become dominant and take the total work into the positive regime.

To clarify the last discussion in Fig.3(a) we show the energy of the first excited state in the hot and cold case, as well as the thermal energy for both reservoirs, where the ground state energy has been set to zero (see appendix A, Fig. 11 for the energy spectrum of the quantum Rabi model for higher states). We can see that E_1^h is always greater than E_1^c which means that the energy difference factor in W_1 is always positive, hence the negative value of W_1 for $g/\omega_c \gtrsim 1.2$ originates from the population difference factor of W_1 . In Fig. 3(b) we plot the thermal population of $|E_1^h\rangle$ (red line) and $|E_1^c\rangle$ (blue line). As we can see, in the region $g/\omega_c \lesssim 1.2$ the population of the hot excited state is greater than that of the cold excited state, and we have $P_1(T_h) - P_1(T_c) > 0$, but for greater values of g/ω_c we have $P_1(T_h) - P_1(T_c) < 0$ which corresponds to the refrigeration regime.

To understand the behavior of the population difference explained above, we look at Fig.3(a) which shows that the ratio $E_1^{c,(h)}/k_B T_{c,(h)}$ decreases monotonously as g/ω_c increases. Near the point of intersection of $E_1^{c,(h)}$ and $k_B T_{c,(h)}$ the thermal population will increase rapidly. This is the role that the anharmonicity and degeneracy between the ground and first excited state play on the behavior of the thermal population and is necessary to have $P_1(T_h) - P_1(T_c) < 0$. However, this is not enough to achieve a refrigeration regime, the missing condition is provided by the adiabatic process. As mentioned before, the adiabatic process makes the ratio g/ω of the hot Hamiltonian to be half the ratio of the cold Hamiltonian, as consequence, E_1^h intersects $k_B T_h$ at a greater value of g/ω_c as compared with its cold counterpart, see Fig.3(a). This leads to

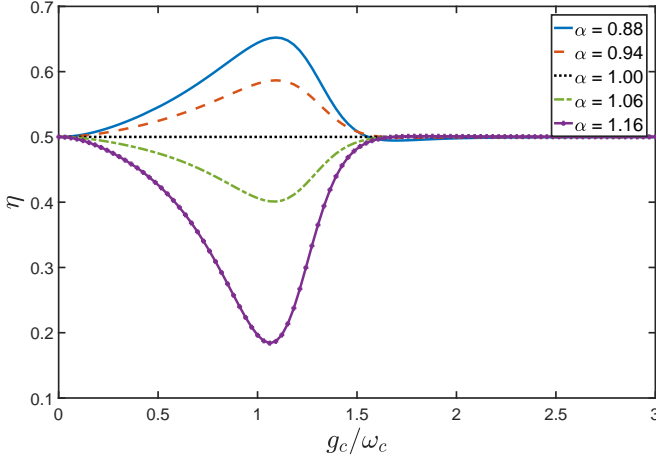


FIG. 6. Efficiency of the QHE for different proportionality constant α versus the light-matter coupling g_c/ω_c . We have used $\omega_h = 2\omega$ and $\omega_c = \omega$, $T_c = 19$ mK and $T_h = 9T_c$.

the negative value of the population difference term in Eq.(7). These two factors, namely, the anharmonicity of the energy spectrum and the specifics of the adiabatic process, give rise to the refrigeration regime.

By following a similar procedure as in Refs. [39, 40] we can obtain an approximated expression for the energy levels, see appendix B, which allow us to derive an approximated positive work condition for W_1 on the ratio g/ω_c

$$\frac{g}{\omega} < \sqrt{\frac{1}{2} \frac{R^2}{R^2 - 1} \ln\left(\frac{1}{R} \frac{T_h}{T_c}\right)}, \quad (9)$$

where $R = \omega_h/\omega_c < T_h/T_c$. From this relation we can obtain an intuition about the effect of the adiabatic process on positive and negative work regime. For a fixed temperature ratio the right-hand side of Eq.(9) is a decreasing function of R and this in turn indicates that an adiabatic process with large R will have a small interval of g/ω_c where the extractable work is positive.

V. QUANTUM CORRELATIONS AND WORK EXTRACTION

We have learned that for the quantum Rabi model as working substance, the system can experience a transition in operation regime depending on the light-matter coupling strength. An important issue to be considered is the study of correlations embedded in hybrid states of the quantum Rabi model, and the role they play in the operation regimes of the QHE. It has been suggested that the quantum correlations that are built at the end of the cold bath stage may be interpreted as a resource for enhancing work extraction [14]. The result that we present in what follows indicates that the difference of quantum correlations between the initial and final state of the hot bath stage is the quantity to be considered as a resource for harvested work.

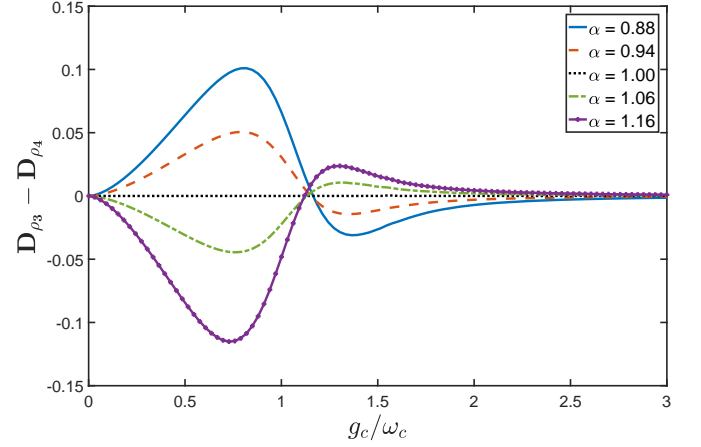


FIG. 7. Difference of quantum correlations between states ρ_3 and ρ_4 for different proportionality constant α , versus the light-matter coupling g_c/ω_c . We have used $\omega_h = 2\omega$ and $\omega_c = \omega$, $T_c = 19$ mK and $T_h = 9T_c$.

We will quantify the quantum correlations between the two-level system and the field mode by means of quantum discord (QD). This measure allows to capture correlations that do not necessarily involve only quantum entanglement.

The quantum discord in a bipartite (A, B) system can be obtained as follows [41]:

$$D_A = S(\rho_A) - S(\rho_{AB}) + \min_{\{\Pi_j^A\}} S(\rho_{B|\{\Pi_j^A\}}), \quad (10)$$

where $S(\rho) = -\text{tr}(\rho \ln \rho)$ is the von Neumann entropy, $\rho_{A,B}$ is the reduced density matrix for subsystem A or B, ρ_{AB} is the density matrix of the complete system, and $\rho_{B|\{\Pi_j^A\}}$ is the state of the complete system after a projective measurement Π_j^A is performed on subsystem A. In our case, the subsystem A will be the two-level system and subsystem B will be the field mode. Due to the size of the Hilbert space of the working substance we perform the projective measurements on the two-level system only. The strategy we use to calculate the optimal conditional entropy is the simulation technique used in Ref.[42]

Which are the states whose quantum correlations should we consider as a resource for work extraction? We know that in the hot bath stage quantum correlations are destroyed while in the cold bath stage correlations are created. On the other hand, the adiabatic compression and expansion processes can significantly change the amount of quantum correlations that are present in the thermal equilibrium states. We can intuitively think that during the hot bath stage the heat provided by the hot reservoir would have to be proportional to the amount of quantum correlations destroyed in this thermalization process. This suggests that the quantum correlations that we should consider are those present in the initial and final states of the hot bath stage.

In order to support the above claim, let us consider the generalized quantum Rabi model with $\theta \neq 0$. In Fig. 4(a) we plot the difference of quantum correlations between the initial and

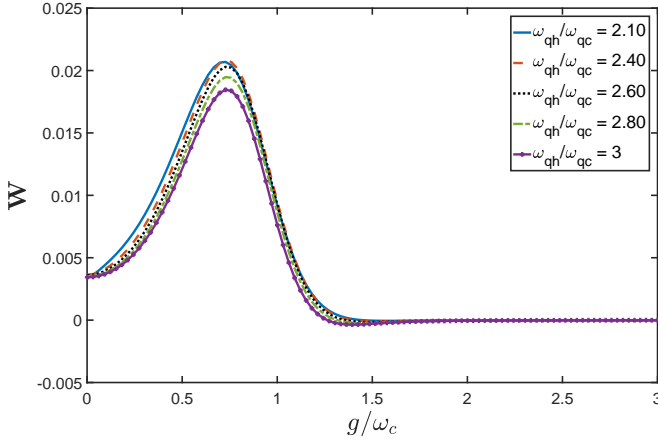


FIG. 8. Work output of the engine versus the coupling parameter g/ω_c for different frequencies ω_{qh} of the hot qubit, where we have fixed $\omega_{qc} = 0.5\omega$. We have considered $T_c = 19\text{mK}$ and $T_h = 4T_c$.

final states (ρ_4 and ρ_1) of the hot bath stage. In Fig. 4(b) we plot the difference of quantum correlations between the cold thermal state ρ_3 and the hot thermal state ρ_1 . Also, in Fig. 5 we plot the extractable work W for different values of the mixing angle θ . If we compare Fig. 4(a) and Fig. 5 we can see that $D_{\rho_4} - D_{\rho_1}$ has a similar profile as the extractable work W in the sense that maxima and minima can be equally identified. In this way, this difference of quantum correlations may be considered as a resource for work extraction. This is not the case for the difference of quantum correlations between the cold thermal state ρ_3 and the hot thermal state ρ_1 as shown in Fig. 4(b). Here, the reduction in quantum correlations is no longer related to the behavior of the extractable work. We conclude that the quantum correlations which act as resource for work extraction are those of the initial and final state of the hot bath stage.

It is noteworthy that for the mixing angle $\theta = 0$, Fig. 4(a) and Fig. 4(b) show the same behavior in accordance with the work extraction. In this case the compression stage does not change the quantum correlations significantly, so ρ_3 and ρ_4 have a very similar amount of quantum correlations. However, as the mixing angle increases the quantum adiabatic processes change the amount of quantum correlations present in the cold thermal state as evidenced by Fig. 4(a). This is the reason why the difference in quantum correlations $D_{\rho_3} - D_{\rho_1}$ cannot be considered as a resource for work extraction.

VI. QUANTUM CORRELATIONS AND EFFICIENCY

Besides the characterization of the harvested work, a complete description of a QHE also requires the study of its efficiency. As the work extraction arises from the adiabatic compression process, it is worthy to ask whether the change of quantum correlations induced by the compression stage is related to the efficiency of the QHE. In what follows, we show that the difference of quantum correlations in the compression stage can be considered a resource for enhanced efficiency of

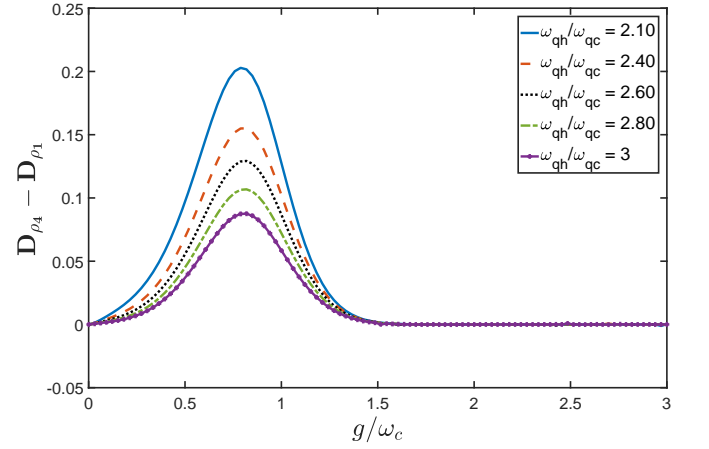


FIG. 9. Difference of quantum correlations between the initial and final state of the hot bath stage as a function of coupling parameter g/ω_c for different frequencies ω_{qh} of the hot qubit, where we have fixed $\omega_{qc} = 0.5\omega$. We have used $\omega_h = \omega_c = \omega$ and $T_c = 19\text{mK}$ and $T_h = 4T_c$.

the QHE.

We will consider an adiabatic process where we change simultaneously the resonator frequency and the coupling strength parameter between the values $\{\omega_c, \omega_h\}$ and $\{g_c, g_h\}$ respectively. Specifically, we will consider an adiabatic process that sets $g_h = \alpha \frac{\omega_h}{\omega_c} g_c$, and study the difference of quantum correlations and efficiency of the QHE as a function of the coupling g_c/ω_c for different values of the parameter α and for a fixed ω_h/ω_c . Here we have included the change of the coupling parameter in our adiabatic process since it allows the hot Hamiltonian H_h to be proportional to the cold Hamiltonian H_c ($\alpha = 1$), and therefore, there is no change of quantum correlations in the compression stage. In Fig. 6 we plot efficiency η versus the coupling g_c/ω_c for different values of the proportionality constant α , in this numerical calculation we use $\omega_c = \omega$, $\omega_h = 2\omega$ and the mixing angle $\theta = 0$ for simplicity. Also in Fig. 7 we plot the difference of quantum correlations between the initial and final state of the compression stage. By comparing Fig. 6 and Fig. 7, we notice that when $\alpha = 1$, that is, when the hot Hamiltonian is proportional to the cold Hamiltonian, the light-matter coupling no longer affects the efficiency of the QHE, and there is no change of quantum correlations in the compression stage. For the case of $\alpha < 1$ we see that there is an optimal coupling region where the efficiency is maximized and it corresponds to the cases where there is a reduction in quantum correlations during the adiabatic compression state. On the other hand, when $\alpha > 1$ the coupling ratio g_c/ω_c has a negative impact on the efficiency in the region where the quantum correlation difference $D_{\rho_3} - D_{\rho_4}$ is negative. These observations allow us to conclude that the difference in quantum correlations between the initial and final states of the compression stage act as resource for enhanced engine efficiency.

These results together with the previous section give us a broader picture of the role of quantum correlations in the performance of the QHE, the quantum correlation reduction dur-

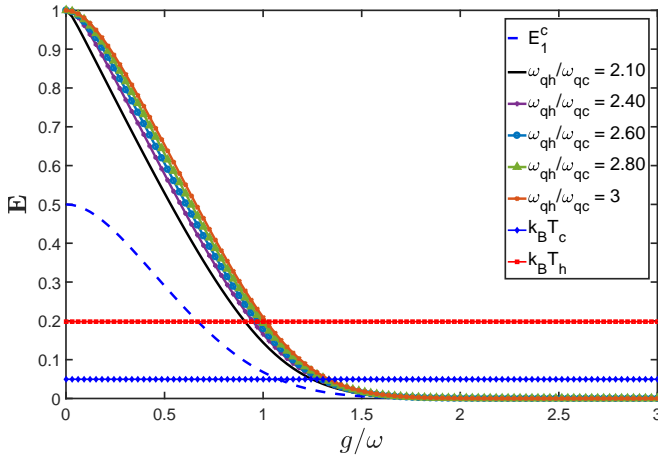


FIG. 10. Energy of the first excited state E_1 for the cold Hamiltonian (blue dashed line), for the hot Hamiltonian for different values of the hot qubit frequency (solid lines) as a function of coupling parameter g/ω . We also show the thermal energy of the hot reservoir (red squares) and cold reservoir (blue diamonds). Where we have used $\omega_{qc} = 0.5\omega$, $T_c = 19\text{mK}$ and $T_h = 4T_c$.

ing the hot isochoric stage acts as resource for harvested work while a quantum correlation reduction during the compression stage is an indicator of the behavior of the engine efficiency.

VII. AN OPTIONAL ADIABATIC PROCESS

In the previous sections we have assumed the control of the coupling with respect to the cold resonator frequency and we have described the regime of operation changing from heat engine into refrigerator. An alternative point of view to analyze our model is to consider, for example, to control only the qubit frequency which can be physically achieved in superconducting platforms by controlling the magnetic field threading a superconducting quantum interference device (SQUID) [43, 44]. In this case the adiabatic stages will only change the frequency of the qubit between the two values ω_{qc} and ω_{qh} , while we fix the resonator frequency and coupling ratio g/ω for the Otto cycle. For the sake of simplicity we will only consider the case of the quantum Rabi model, that is the mixing angle $\theta = 0$.

In Fig. 8 we plot the work output of the engine for different frequencies ω_{qh} of the two-level system in the hot Hamilto-

nian, and in Fig. 9 we plot the corresponding difference of quantum correlations measured as quantum discord between the initial and final state of the hot bath stage. As can be seen from both figures, we still see the same relation between extractable work and the reduction of quantum correlations that happens in the hot bath stage. In this case the quantum correlations in the hot thermal state are never greater than those present in ρ_3 and we observe only heat engine operation.

The absence of refrigeration regime, as compared with the results obtained in section IV, can be understood from Fig. 10 where we plot the energy of the first excited state of the quantum Rabi model for the different frequencies of the hot qubit. As can be seen from the figure, the energy of the hot first excited state intersects the hot thermal energy $k_B T_h$ in a smaller value of the ratio g/ω_c as compared with the cold first excited state and the cold thermal energy $k_B T_c$. As a consequence the thermal population of the hot first excited state will always be greater than its cold counterpart. Therefore, both terms of Eq. (7) are positive and we can conclude that this adiabatic process does not allow refrigeration regime.

VIII. CONCLUSIONS

We have shown how the anharmonicity and degeneracy of the spectrum of the quantum Rabi model give rise to an operation regime transition from heat engine into refrigerator as the light-matter coupling increases. By considering a generalized quantum Rabi model we found that the quantum correlations reduction in the hot bath stage and in the compression stage of the cycle can lead to enhanced positive work extraction and efficiency respectively. We have also shown that an alternative adiabatic process for the quantum Rabi model still maintains the relation we have shown between quantum correlations and positive work extraction, and may be implemented with the state-of-the-art circuit QED. Our results shed light on the search for optimal conditions in the performance of coupled quantum heat engines in relation to the properties of the energy spectrum and the capability of the working substance for embedding quantum correlations.

Acknowledgements. G.A.B acknowledges support from CONICYT Doctorado Nacional 21140587, F.A.-A acknowledges support CONICYT Doctorado Nacional 21140432, F.A.C.-L acknowledges support from CEDENNA basal grant No. FB0807 and Dirección de Postgrado USACH, G.R acknowledges the support from FONDECYT under grant No. 1150653 and J. C. R acknowledges the support from FONDECYT under grant No. 1140194.

-
- [1] H. E. D. Scovil and E. O. Schulz-DuBois, *Phys. Rev. Lett.* **2**, 262 (1959).
 - [2] T. Feldmann, E. Geva, R. Kosloff, and P. Salamon, *American Journal of Physics* **64**, 485 (1996).
 - [3] T. Feldmann and R. Kosloff, *Phys. Rev. E* **70**, 046110 (2004).
 - [4] Y. Rezek and R. Kosloff, *New Journal of Physics* **8**, 83 (2006).
 - [5] M. J. Henrich, F. Rempp, and G. Mahler, *The European Physi-*

cal Journal Special Topics **151**, 157 (2007).

- [6] H. T. Quan, Y.-x. Liu, C. P. Sun, and F. Nori, *Phys. Rev. E* **76**, 031105 (2007).
- [7] J. He, X. He, and W. Tang, *Science in China Series G: Physics, Mechanics and Astronomy* **52**, 1317 (2009).
- [8] G. Thomas, M. Banik, and S. Ghosh, arXiv preprint arXiv:1607.00994 (2016).

- [9] J. He, J. Chen, and B. Hua, *Phys. Rev. E* **65**, 036145 (2002).
- [10] E. Geva, *The Journal of Chemical Physics* **104**, 7681 (1996).
- [11] S. Li, H. Wang, Y. D. Sun, and X. X. Yi, *Journal of Physics A: Mathematical and Theoretical* **40**, 8655 (2007).
- [12] C. M. Bender, D. C. Brody, and B. K. Meister, *Proceedings of the Royal Society of London A: Mathematical, Physical and Engineering Sciences* **458**, 1519 (2002).
- [13] R. Kosloff and Y. Rezek, *Entropy* **19** (2017).
- [14] F. Altintas, A. U. C. Hardal, and O. E. Müstecaplıoğlu, *Phys. Rev. A* **91**, 023816 (2015).
- [15] Q. Song, S. Singh, K. Zhang, W. Zhang, and P. Meystre, *Phys. Rev. A* **94**, 063852 (2016).
- [16] T. Zhang, W.-T. Liu, P.-X. Chen, and C.-Z. Li, *Phys. Rev. A* **75**, 062102 (2007).
- [17] G. F. Zhang, *The European Physical Journal D* **49**, 123 (2008).
- [18] H. Wang, S. Liu, and J. He, *Phys. Rev. E* **79**, 041113 (2009).
- [19] R. Dillenschneider and E. Lutz, *EPL (Europhysics Letters)* **88**, 50003 (2009).
- [20] F. Altintas, A. U. C. Hardal, and O. E. Müstecaplıoğlu, *Phys. Rev. E* **90**, 032102 (2014).
- [21] T. Niemczyk, F. Deppe, H. Huebl, E. Menzel, F. Hocke, M. Schwarz, J. García-Ripoll, D. Zueco, T. Hümmer, E. Solano, *et al.*, *Nature Physics* **6**, 772 (2010).
- [22] P. Forn-Díaz, J. Lisenfeld, D. Marcos, J. J. García-Ripoll, E. Solano, C. J. P. M. Harmans, and J. E. Mooij, *Phys. Rev. Lett.* **105**, 237001 (2010).
- [23] J. Bourassa, J. M. Gambetta, A. A. Abdumalikov, O. Astafiev, Y. Nakamura, and A. Blais, *Phys. Rev. A* **80**, 032109 (2009).
- [24] F. Yoshihara, T. Fuse, S. Ashhab, K. Kakuyanagi, S. Saito, and K. Semba, *Nature Physics* **13**, 44 (2017).
- [25] P. Forn-Díaz, J. García-Ripoll, B. Peropadre, J.-L. Orgiazzi, M. Yurtalan, R. Belyansky, C. Wilson, and A. Lupascu, *Nature Physics* **13**, 39 (2017).
- [26] F. Yoshihara, T. Fuse, S. Ashhab, K. Kakuyanagi, S. Saito, and K. Semba, *Phys. Rev. A* **95**, 053824 (2017).
- [27] I. I. Rabi, *Phys. Rev.* **51**, 652 (1937).
- [28] D. Braak, *Phys. Rev. Lett.* **107**, 100401 (2011).
- [29] P. Nataf and C. Ciuti, *Phys. Rev. Lett.* **107**, 190402 (2011).
- [30] G. Romero, D. Ballester, Y. M. Wang, V. Scarani, and E. Solano, *Phys. Rev. Lett.* **108**, 120501 (2012).
- [31] T. H. Kyaw, S. Felicetti, G. Romero, E. Solano, and L.-C. Kwek, *Scientific Reports* **5**, 8621 (2015).
- [32] T. H. Kyaw, D. A. Herrera-Martí, E. Solano, G. Romero, and L.-C. Kwek, *Phys. Rev. B* **91**, 064503 (2015).
- [33] C. Joshi, E. K. Irish, and T. P. Spiller, *Scientific Reports* **7**, 45587 (2017).
- [34] F. A. Wolf, F. Vallone, G. Romero, M. Kollar, E. Solano, and D. Braak, *Phys. Rev. A* **87**, 023835 (2013).
- [35] D. Z. Rossatto, C. J. Villas-Bôas, M. Sanz, and E. Solano, arXiv preprint arXiv:1612.03090 (2016).
- [36] E. T. Jaynes and F. W. Cummings, *Proceedings of the IEEE* **51**, 89 (1963).
- [37] J. Casanova, G. Romero, I. Lizuain, J. J. García-Ripoll, and E. Solano, *Phys. Rev. Lett.* **105**, 263603 (2010).
- [38] T. D. Kieu, *Phys. Rev. Lett.* **93**, 140403 (2004).
- [39] E. K. Irish, *Phys. Rev. Lett.* **99**, 173601 (2007).
- [40] L. Yu, S. Zhu, Q. Liang, G. Chen, and S. Jia, *Phys. Rev. A* **86**, 015803 (2012).
- [41] A. Datta and S. Gharibian, *Phys. Rev. A* **79**, 042325 (2009).
- [42] S. Allende, D. Altbir, and J. C. Retamal, *Phys. Rev. A* **92**, 022348 (2015).
- [43] F. G. Paauw, A. Fedorov, C. J. P. M. Harmans, and J. E. Mooij, *Phys. Rev. Lett.* **102**, 090501 (2009).
- [44] M. J. Schwarz, J. Goetz, Z. Jiang, T. Niemczyk, F. Deppe,

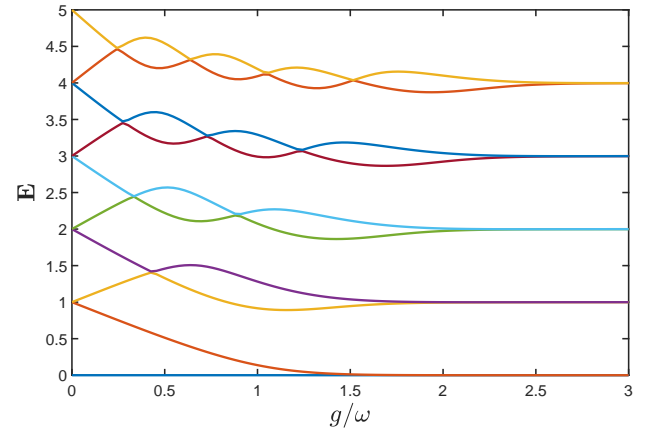


FIG. 11. Energy spectrum of the quantum Rabi model relative to the ground state as a function of coupling parameter g/ω .

A. Marx, and R. Gross, *New Journal of Physics* **15**, 045001 (2013).

Appendix A: Energy spectrum of the quantum Rabi model

The quantum Rabi model described by the Hamiltonian

$$H = \hbar \frac{\Omega}{2} \sigma_z + \hbar \omega a^\dagger a + \hbar g \sigma_x (a^\dagger + a), \quad (\text{A1})$$

has been studied elsewhere. Here, we focus on the anharmonicity of its energy spectrum which is shown in Fig.11 as a function of the ratio g/ω . All the physics explained in this article is well captured by the ground and first excited state of the quantum Rabi model.

Appendix B: Approximation for the energies of the quantum Rabi model

In order to compute the eigenenergies of the quantum Rabi model we follow Refs. [39, 40]. In particular, we write the quantum Rabi model in a form which allows an expansion in terms of the creation and annihilation operators. This expression can be truncated to obtain a diagonalizable Hamiltonian that leads to the approximated energy levels of the quantum Rabi model, this in turn will allow us to derive the positive work condition of Eq.(9).

We proceed by rotating the two-level system such that the QRM can be written as:

$$H = \hbar \omega a^\dagger a - \hbar \frac{\Omega}{2} \sigma_x + \hbar g (a^\dagger + a) \sigma_z. \quad (\text{B1})$$

Next, we apply the displacement operator $D(g/\omega) =$

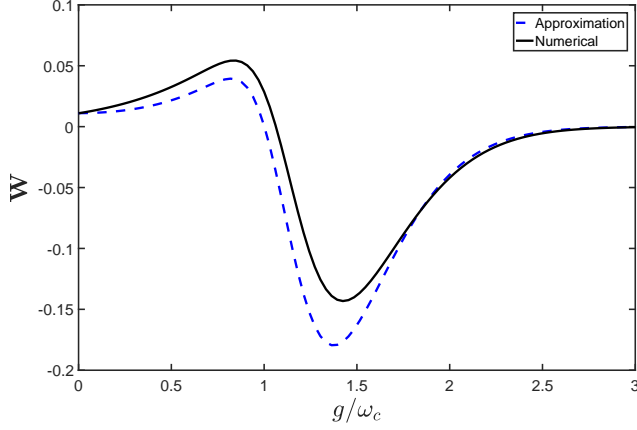


FIG. 12. Work contribution of the first excited state W_1 as obtained by the approximation presented (blue-dashed line) compared with the numerically-determined values (solid black line). Where we have used $T_c = 19\text{mK}$ and $T_h = 9T_c$.

$\exp(\frac{g}{\omega}\sigma(a^\dagger - a))$ and obtain

$$H_2 \equiv DHD^\dagger = \hbar\omega a^\dagger a - \hbar\frac{g^2}{2} - \hbar\frac{\Omega}{2}e^{-\frac{2g^2}{\omega^2}} \begin{pmatrix} 0 & e^{\frac{2g}{\omega}a^\dagger}e^{-\frac{2g}{\omega}a^\dagger} \\ e^{-\frac{2g}{\omega}a^\dagger}e^{\frac{2g}{\omega}a^\dagger} & 0 \end{pmatrix}. \quad (\text{B2})$$

Now expanding the exponential operators as

$$e^{\frac{2g}{\omega}a^\dagger}e^{-\frac{2g}{\omega}a^\dagger} = \sum_{n,m} \frac{(2g/\omega)^n a^{\dagger n}}{n!} (-1)^m \frac{(2g/\omega)^m a^m}{m!}, \quad (\text{B3})$$

the Hamiltonian becomes:

$$H_3 = \hbar\omega a^\dagger a - \hbar\frac{g^2}{\omega} - \hbar\frac{\Omega}{2}e^{-2\frac{g^2}{\omega^2}}\Theta\sigma_x - \hbar\frac{g}{\omega}\Omega e^{-2\frac{g^2}{\omega^2}}(a^\dagger A - Aa)(\sigma_+ - \sigma_-) + \dots \quad (\text{B4})$$

where

$$\Theta = \sum_{n=0}^{\infty} \frac{(-1)^n (\frac{2g}{\omega})^{2n}}{(n!)^2} a^{\dagger n} a^n$$

$$A = \sum_{n=0}^{\infty} \frac{(-1)^n (\frac{2g}{\omega})^{2n+1}}{n!(n+1)!} a^{\dagger n} a^n. \quad (\text{B5})$$

We recognize the last term of Eq.(B4) as an interaction term which is exponentially damped by a factor $e^{-2\frac{g^2}{\omega^2}}$, this justifies the application of the RWA and leads to a diagonalization of H_3 in a similar way as for the Jaynes-Cummings Hamiltonian. However, we seek a simple expression for the approximated energies of H , thus we shall only consider the free term of Eq.(B4), that is:

$$H_4 = \hbar\omega a^\dagger a - \hbar\frac{g^2}{\omega} - \hbar\frac{\Omega}{2}e^{-2\frac{g^2}{\omega^2}}\Theta\sigma_x. \quad (\text{B6})$$

Now, the eigenstates of the above Hamiltonian are of the form $|\pm, n\rangle$, with energies:

$$E_{\pm, n} = -\hbar\omega n - \hbar\frac{g^2}{\omega} \mp \hbar\frac{\Omega}{2}e^{-2\frac{g^2}{\omega^2}}L_n(4\frac{g^2}{\omega^2}), \quad (\text{B7})$$

where $L_n(4\frac{g^2}{\omega^2})$ is a Laguerre polynomial of order n . Then the energy of the ground and first excited states are:

$$E_G = -\hbar\frac{g^2}{\omega} - \hbar\frac{\Omega}{2}e^{-2\frac{g^2}{\omega^2}} \quad (\text{B8})$$

$$E_1 = -\hbar\frac{g^2}{\omega} + \hbar\frac{\Omega}{2}e^{-2\frac{g^2}{\omega^2}}. \quad (\text{B9})$$

Now we can obtain an approximated expression for the work contribution of the first excited state W_1 , which dominates the behavior of the harvested work. We choose $\omega_h = \Omega_h = R\omega$ and $\omega_c = \Omega_c = \omega$, and write the inverse temperatures for the cold and hot reservoir as $\beta_h = 1/k_B T_h$ and $\beta_c = 1/k_B T_c$. Then, for a two-level approximation, Eq.(5) of the main text reads

$$W = (b_h - b_c)(\tanh(\beta_c b_c) - \tanh(\beta_h b_h)), \quad (\text{B10})$$

where $b_h = \hbar\frac{R\omega}{2}e^{-2\frac{g^2}{R^2\omega^2}}$, $b_c = \hbar\frac{\omega}{2}e^{-2\frac{g^2}{\omega^2}}$ and $R = \frac{\omega_h}{\omega_c} > 1$.

Figure 12 shows W_1 as calculated from Eq.(B10) compared with the numerical calculation. As can be seen, while the difference between the approximation and the numerical calculation cannot be neglected, it is clear that Eq.(B10) captures the behavior of W_1 . Now, from Eq.(B10) we can obtain the condition for the positive work regime by imposing $W > 0$, which leads to

$$\frac{T_h}{T_c} > \frac{\omega_h}{\omega_c}e^{2\frac{g^2}{\omega^2}(1-\frac{1}{R^2})}. \quad (\text{B11})$$

We can also express the above equation as follows

$$\frac{g}{\omega} < \sqrt{\frac{1}{2}\frac{R^2}{R^2-1}\ln\left(\frac{1}{R}\frac{T_h}{T_c}\right)}. \quad (\text{B12})$$